Bridging 1D System Modeling and 3D CFD for Hydraulic Slack Adjuster Design: A Decoupled Co-Simulation Approach

Vignesh Jeganathan[1,*], Chris Imholte[2], Ashutosh Pandey[1], Bipin Kashid[2]

[1]*Simerics, Inc.*
[2]*Parker Hannifin Corporation*
[*]*Corresponding Author, E-mail:* vj@simerics.com

Abstract

The design of safety-critical hydraulic braking subsystems, such as slack adjusters, necessitates the accurate prediction of complex transient interactions between multi-body kinematics and high-fidelity fluid dynamics. While traditional one-dimensional (1D) lumped-parameter models offer system-level insights, they fail to resolve localized phenomena like cavitation, flow separation, and transient pressure spikes. Conversely, fully coupled 3D computational fluid dynamics (CFD) is often computationally prohibitive for extensive design-space exploration. This paper proposes a technically robust, decoupled 1D-3D co-simulation methodology that leverages the strengths of both modeling paradigms to optimize hydraulic performance and reliability. In the proposed framework, a 1D system model is utilized to perform a comprehensive parametric study across a wide range of operating pressures and accumulator configurations, identifying critical transients and near-failure edge cases. These 1D-derived results are then mapped as time-dependent boundary conditions to a high-fidelity 3D CFD model within the Simerics MP environment. A novel contribution of this work is the implementation of a tailored modeling strategy for multi-body fluid-structure interaction (FSI), where contact formulations and damping factors—guided by 1D kinematic data—are used to stabilize the simulation of rapid cylinder collisions. The re-

River Journal, 1–20.

sults indicate that the decoupled approach resolves complex flow and pressure interactions driven by component geometry, which are not captured by one dimensional analysis, yet preserves acceptable computational overhead. This methodology provides a scalable framework for industrial design teams to shorten development cycles and enhance the robustness of complex hydraulic systems through early-stage detection of failure modes.

Keywords: Slack Adjuster, Brakes, Computational Fluid Dynamics, Valve Body collision.

1 Introduction

The hydraulic slack adjuster is a multi-component device designed to maintain a consistent, predetermined residual pressure downstream of the device following the decay of an upstream input [1]. This residual pressure ensures that a finite trapped fluid volume persists within the braking caliper circuit, which in turn preserves a controlled offset distance between the brake pad and rotor interface [2]. The functional consequence of this offset is repeatable, reliable brake engagement and consistent pedal feel at the operator input interface [3].

The primary structural element of the device is a hydraulically balanced valve bodies, effectively an equal-area cylinder with custom end caps, that is spring-biased toward the downstream end cap [4]. This configuration divides the internal volume into two hydraulically distinct regions, as shown in figure. 1. The upstream region, referred to as the apply side, receives pressure input from a controlling brake valve. The downstream region, interfaces directly with the hydraulic braking caliper also referred as accumulator, due to model similarity. Under normal apply conditions, pressure is communicated across Body 1 via a check valve, which permits flow from the upstream brake valve input to the accumulator region whenever a positive pressure differential exists in that direction.

The trapping and release of accumulator volume is governed by a two-component sub-assembly consisting of a remote pressure-referenced sliding piece Body 3 and a floating component, Body 2. Body 3 uses atmospheric reference pressure on one face and upstream supply pressure on the opposing face. When upstream pressure rises sufficiently above atmospheric, the sliding piece displaces to the right, no longer interacting mechanically with the floating Body 2. Under normal conditions, Body 2 is seated against Body 1, sealing the accumulator region from the upstream region. A pressure differen-

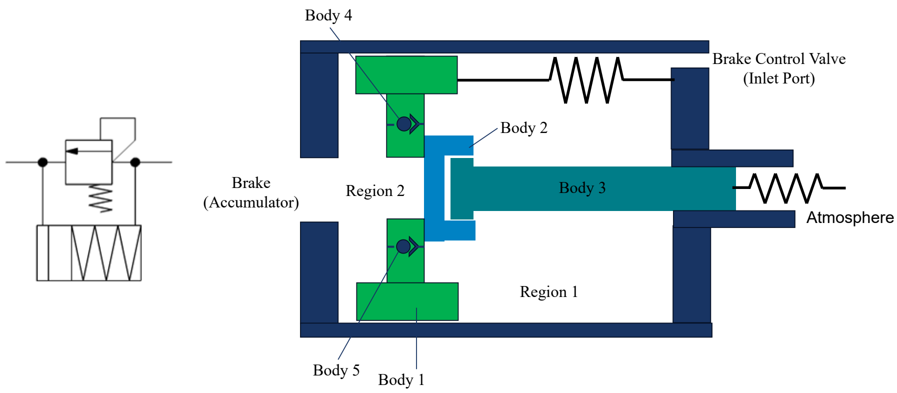

Figure 1 Body 1 denotes a rodless cylinder with equal areas, biased by a spring. Bodies 2 and 3 denote a modified form of a sequence valve. Body 4 consists of ball valves that permit one-way flow from region 1 to region 2. Collision and separation of these bodies 1,2 and 3 opens or closes fluid channels between the regions 1 and 2.

tial of sufficient magnitude unseats the Body 2, permitting accumulator fluid to return to the Brake Control Valve, which occurs during brake release. Once the Body 3 senses that upstream pressure has dropped equal to the spring force, it displaces back to the left, returning Body 2 to its fully seated position and sealing the accumulator volume. The resulting pressure difference across the Body 1 is then sufficient to produce Body 1 displacement to the right, with the system reaching force equilibrium.

Design-space exploration for this mechanism is governed less by the isolated performance of individual components and more by the timing and sequencing of interactions between them. The critical event is the sealing of trapped accumulator volume at a specified upstream pressure threshold, which initiates the Body 1 motion responsible for slack absorption. Two distinct failure modes bound the acceptable design space. If the Body 2 seals late, the trapped volume and corresponding pressure rise are insufficient to achieve full Body 1 stroke to the right; in the limiting case, no slack is absorbed and the braking device does not function as intended. Conversely, premature sealing prevents adequate reduction of accumulator pressure prior to brake release, resulting in residual caliper engagement and a separate class of functional failure where the brake rotors do not disengage. The design space is therefore defined by acceptable timing windows rather than single steady-state performance targets.

Within this timing-governed framework, the relevant design parameters are the spring rates and area ratios of the pressure-referenced sliding piece (Body 3), the spring rates and available displacement of the spring biasing Body 1, and the geometric relationship between the sliding piece and Body 2 that determines the mechanical interaction. These parameters interact such that no single component can be sized independently; the area ratio sets the pressure at which the sliding piece actuates, which in turn determines when Body 2 is driven to reseat, and the spring must provide sufficient restoring force over the available stroke to complete sealing under worst-case pressure decay conditions. Bounding this parameter space through 1D simulation prior to hardware fabrication is therefore essential for risk reduction.

For a given Body 1 bore area and required stroke, there exists a minimum sealed volume below which the residual trapped pressure rise is to deliver the net force required for full displacement. When the trapped volume falls below this threshold, the accumulator pressure decreases to equilibrium before Body 1 completes its stroke, and the lack of absorption is incomplete. The robust design therefore requires that the nominal trapped volume be sized with sufficient margin above this threshold to accommodate the combined worst-case contributions of leakage and mechanical load variation across the full operating envelope.

The 1D lumped-parameter model provides an effective and computationally efficient tool for system-level design-space exploration, timing assessment, and parametric sensitivity studies. However, the governing physics of the Body 2 sub-assembly include several locally three-dimensional phenomena that are not reliably captured within a lumped formulation, and which are consequential to the accurate prediction of device timing and dynamic stability [5].

The Body 2 features a unique surface profile and seat geometry that produces strong spatial gradients in pressure and velocity in the near-seat region due to geometry space limitations. The net axial hydraulic force acting on the Body 2 is highly sensitive to the instantaneous development of the flow jet, the location of flow separation from the seat geometry, and the degree of pressure recovery accumulator of the minimum flow area. These effects are collectively sensitive to the mass ratio of the moving element and to the precise geometric transition through small lift values. In a 1D representation, these phenomena are necessarily collapsed into a single effective flow area and a lumped jet force coefficient, which cannot capture the variation in net force with lift or the potential for flow-force-induced instability in the low-lift regime beyond a single component.

Additionally, the leakage behavior of the assembly is governed by multiple lift-dependent flow paths defined by the proximity of complex mating surfaces. The controlling restriction along these paths can shift between geometric features edges and clearance gaps as the Body 2 moves, and the resulting flow may be transitional with significant viscous influence at small clearances. 1D simulation without physical test data of Body 2 performance cannot represent the migration of the controlling restriction or the associated changes in effective leakage area with lift. The valve timing and fluid damping behavior are similarly influenced by the transient filling and emptying of local volumes adjacent to the Body 2 and by the unsteady pressure field generated during rapid seating events. As such, the moving boundaries, transient jet development, and viscous damping through narrow passages require spatially resolved simulation to predict reliably. Three-dimensional CFD resolves the pressure distribution across the Body 2 surface at each instant, enabling accurate computation of flow forces and leakage as functions of lift, pressure differential, and fluid state. This level of fidelity is necessary to bound the sensitivity of device timing to geometry-driven effects that the 1D model cannot resolve, and to provide confidence that the predicted operating mode, successful slack absorption versus failure, is robust to geometric and operating condition variation.

2 Decoupled Co-Simulation Framework

A fully coupled, time-resolved co-simulation between a system-level 1D model and a transient 3D CFD solver is computationally prohibitive for iterative design analysis. The indirect coupling framework adopted here separates the two modeling domains by leveraging the inherent time-scale and spatial-scale separation between system-level sequencing behavior and local component physics. The 1D model is used to generate transient boundary condition histories such as pressures, flow rates, and component state sequences across the operating envelope. These boundary conditions are then applied to targeted 3D CFD simulations of the Body 2 sub-assembly, which resolve the local flow physics that cannot be represented in the lumped formulation. The two models are not solved simultaneously; rather, results are exchanged in a defined, structured manner that preserves physical consistency while enabling each model to be applied where it is most effective.

This approach is motivated by industrial practicality. The 1D model can be exercised rapidly across large parameter spaces, making it suitable for design-space exploration, sensitivity studies, and identification of candidate operating points that represent edge conditions or failure-adjacent scenarios. The 3D CFD model is then applied selectively to those conditions, providing high-fidelity resolution of the local physics at the cases most relevant to design risk. The result is a workflow that achieves the predictive capability of 3D CFD where it is needed without incurring the computational cost of full-envelope 3D simulation.

The boundary condition mapping procedure translates the time-resolved outputs of the 1D model into inlet and outlet pressure or flow rate histories suitable for driving the 3D CFD domain. Key outputs extracted from the 1D simulation include the upstream apply-side pressure trace, the accumulator caliper circuit pressure, and the predicted state sequence of the Body 2 and sliding piece specifically, the timing of Body 2 unseating, the duration of the open flow period, and the predicted reseat event. These traces establish the expected operating window for the transient CFD simulation.

Validation of the co-simulation framework does not seek pointwise quantitative agreement between 1D and 3D results across all outputs. Instead, consistency is assessed against a structured set of behavioral criteria that collectively confirm whether the two models predict the same operating mode and whether discrepancies identify specific physical mechanisms requiring higher-fidelity representation. The first criterion is general displacement agreement: whether the 1D and 3D models both predict Body 1 displacement, or both predict failure to displace, for a given set of boundary conditions. This high-level consistency check validates that the dominant force balance of pressure acting on Body 1 area against spring and mechanical load is captured correctly at the system level, and that the continuity and compressibility accounting in the 1D model is adequate for the purpose of mode prediction. The second criterion addresses leakage representation. In the 1D model, leakage across the Body 3 annular region is represented by an equivalent restriction characterized by an effective area and laminar leakage with varying length leakage assumption. The 3D CFD model resolves the actual evolving gap geometry and viscous pressure loss along the leakage path. Consistency in the rate and shape of accumulator pressure decay between the two models supports the adequacy of the 1D restriction parameterization.

The third criterion is Body 2 reseal behavior. Reseal is governed by the net force balance on the Body 2 as the upstream pressure decays to the atmospheric reference threshold. The 1D model predicts reseal using lumped pressures and simplified hydraulic force assumptions. The 3D CFD simulation reveals whether the near-seat flow field generates stabilizing or destabilizing axial forces at low lift and whether residual leakage through the

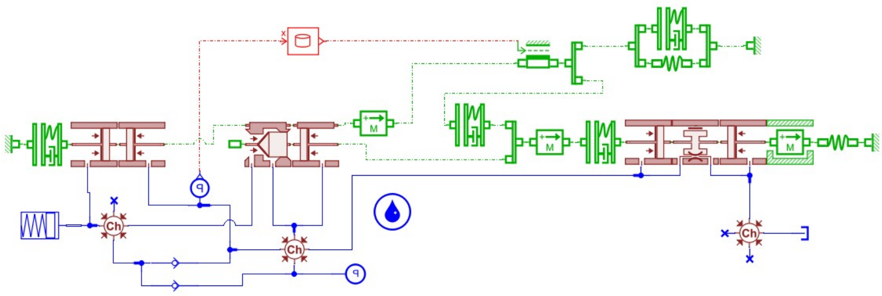

Figure 2 Configuration of the 1D simulation model in modeling software.

shrinking gap inhibits the pressure recovery necessary for complete seating. Agreement in reseal timing and completeness between the two models increases confidence in the sign and magnitude of the dominant modeled forces; disagreement identifies conditions under which flow-force nonlinearity or transient damping effects must be represented with higher fidelity to bound the design space reliably.

The fourth criterion is event sequencing and relative timing. The key event markers such as onset of Body 2 unseating, duration of open flow period, initiation of Body 1 motion, peak trapped-volume pressure, reseal time, and accumulator pressure recovery are compared between the 1D and 3D results. The 1D model provides efficient causal sequence prediction across parameter sets; the 3D model provides a higher-fidelity depiction of the transient pressure evolution associated with real leak-path geometry and jet development. Modest timing offsets between the two models are treated as diagnostic information rather than validation failures, indicating the degree to which lift-dependent leakage, transient damping, or flow-force nonlinearity is driving sequencing sensitivity and therefore must be resolved at higher fidelity to support robust design decisions. Upon iteration it results in a decoupled co-simulation loop of 1D simulation to 3D simulation, where the next iteration utilizes improved parameters for leakage, damping or other parameters.

3 1D simulations

The co-simulation framework described in Section 2 is exercised against a set of targeted case studies selected to expose operating conditions at or near the boundaries of acceptable device performance. 1D simulations are carried out using the simulation setup shown in figure 2. These cases were chosen

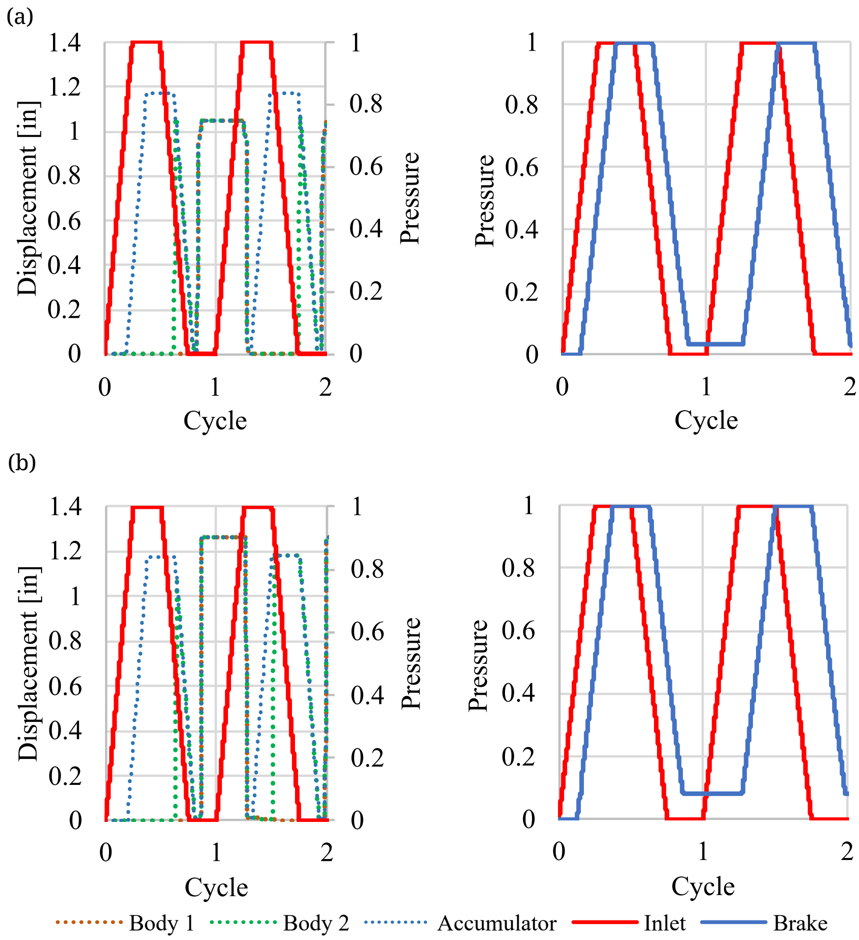

Figure 3 Valve body motion and accumulator (brake) pressure under different inlet pressure cycles for (a) the initial accumulator volume and (b) twice the accumulator volume. Time is non-dimensionalized using cycle time and pressure is normalized by the highest pressure used in the inlet.

specifically because they represent failure modes or edge conditions that are not fully observable in the 1D model alone, and for which the 3D CFD results provide either confirmation or refinement of the predicted system behavior.

3.1 Minimum Trapped Volume for Full Displacement of Body 1

As established in Section 2, there exists a minimum sealed accumulator volume below which the pressure remaining during the trapping event is insufficient to drive the Body 1 to full stroke. This case study independently examines the sensitivity of Body 1 displacement to trapped volume and minimum reapplication pressure. The 1D model was used to sweep the relevant parameters such as accumulator pressure decay rate, and minimum input pressure to identify the boundary conditions under which the predicted trapped volume approaches the minimum displacement threshold.These boundary condition sets are now prepared for implementation in the 3D CFD model to evaluate whether the locally resolved leakage behavior and the evolution of transient pressure align with the 1D predictions at the threshold condition. Of particular interest is whether the 1D equivalent restriction model adequately represents leakage at the low pressure differentials characteristic of the late stages of the trapping event, where small differences in leakage rate have the greatest influence on the final sealed volume. Results from this case study, per figure 2, inform the required volume margin in the nominal design and identify which operating condition variables contribute most significantly to the displacement risk. These findings directly support the sizing guidance established during design-space exploration and provide a quantified basis for design robustness decisions.

In addition, due to the stored energy within the slack adjuster Body 1 upon displacement, there is a minimum apply pressure required to return the Body 1 to the no displacement location. As seen in figure 4a, the slack adjuster has been sized to require 5 bar of brake valve pressure (barring losses) to effectively return the Body 1 to zero displacement (no slack volume). This minimum brake valve pressure input to completely return the Body 1 is a requirement driven through the brake valve subsystem which converts brake command into hydraulic actuation. Effectively sizing this pressure in relation to the constraint represents the minimum pedal displacement from an operator and as such is critical to determine.

3.2 Excessive Leakage Across the Body 3

The annular leakage path associated with the sliding piece Body 3 represents a critical interface in the device. Under nominal conditions, leakage through this path is bounded by the clearance geometry and fluid viscosity, and its effect on trapped volume integrity is accounted for in the 1D model through an equivalent restriction. However, under conditions of elevated clearance,

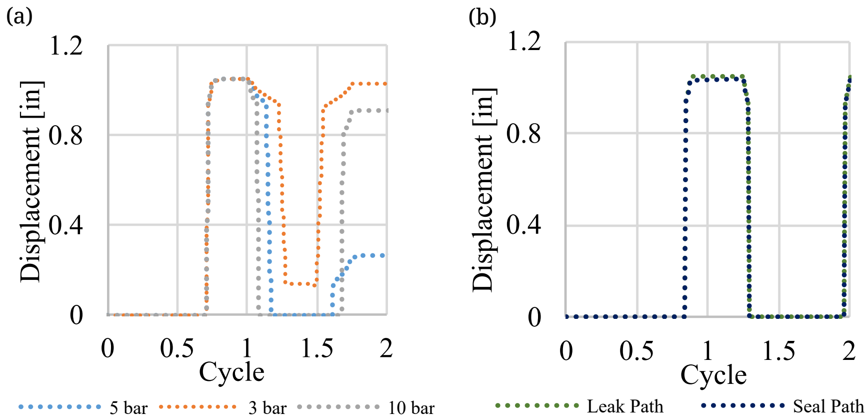

Figure 4 (a) Parametric study of constant caliper volume for various brake valve apply pressures. (b) Displacement of piston that retains slack volume for various leakage amount around the Body 3. Time is non-dimensionalized using cycle time.

arising from manufacturing tolerance stack-up, thermal expansion, or wear, the leakage rate can increase to the point where the force balance is disrupted by local effects or flow rate is of unacceptable magnitude.

In an ideal configuration, a frictionless seal would be represented such that no interface exists between the external atmospheric reference and the upstream pressure. A further development of the model is to incorporate either seal friction or annular leakage. For the present case, the seal was omitted, as illustrated in figure 4b, because a seal failure would exhibit a behavior analogous to that of significant annular leakage.

4 3D Simulations

After performing multiple 1D analyses, we identified a failure mode that must be investigated using Computational Fluid Dynamics (CFD). The modeling process includes defining suitable numerical setups to capture flow phenomena such as cavitation, turbulence, and leakage. Additionally, collision events are modeled carefully to determine valve timing with high accuracy. Significant effort has been devoted to achieving an optimal mesh and timestep size for the 3D CFD simulations.

4.1 Computational Fluid Dynamics model

In a CFD simulation, the Navier–Stokes equations that describe fluid motion are solved numerically to obtain the velocity and pressure fields within the domain.

The spatially averaged conservation equations for mass and momentum can be expressed in integral form as:

$$\frac{\partial}{\partial t}\int_{\Omega(t)} \rho \, d\Omega + \int_{\sigma} \rho(v - v_{\sigma}) \cdot n \, d\sigma = 0, \tag{1}$$

and

$$\frac{\partial}{\partial t}\int_{\Omega(t)} \rho v \, d\Omega + \int_{\sigma} \rho v \big((v - v_{\sigma}) \cdot n\big) d\sigma = \int_{\sigma} \tau \cdot n \, d\sigma - \int_{\sigma} P n \, d\sigma + \int_{\Omega} f \, d\Omega. \tag{2}$$

In the equations above, ρ denotes the density of the working fluid, v is the spatially averaged velocity vector, v_{σ} is the velocity of the moving reference frame, τ is the deviatoric stress tensor, P is the pressure, and f represents the body force, such as gravity. The symbols σ and Ω under the integral signs denote surface and volume integrals, respectively.

Turbulence is modeled using the standard $\kappa - \epsilon$ two-equation model together with a wall function, expressed as:

$$\frac{\partial}{\partial t}\int_{\Omega(t)} \rho\kappa \, d\Omega + \int_{\sigma} \rho\big((v - v_{\sigma}) \cdot n\big)\kappa \, d\sigma = \int_{\sigma} \left(\mu + \frac{\mu_t}{\sigma_{\kappa}}\right) (\nabla\kappa \cdot n) \, d\sigma + \int_{\Omega} (G_t - \rho\epsilon) \, d\Omega, \tag{3}$$

and

$$\frac{\partial}{\partial t}\int_{\Omega(t)} \rho\epsilon \, d\Omega + \int_{\sigma} \rho\big((v - v_{\sigma}) \cdot n\big)\epsilon \, d\sigma = \int_{\sigma} \left(\mu + \frac{\mu_t}{\sigma_{\epsilon}}\right) (\nabla\epsilon \cdot n) \, d\sigma + \int_{\Omega} \left(c_1 G_t \frac{\epsilon}{\kappa} - c_2 \rho \frac{\epsilon^2}{\kappa}\right) d\Omega. \tag{4}$$

Here, κ denotes the spatially averaged turbulent kinetic energy, ϵ the spatially averaged dissipation rate of turbulent kinetic energy, μ_t the turbulent (eddy) viscosity, c_1 and c_2 are closure constants of the model, and G_t is the production term of turbulent kinetic energy.

To represent cavitation and aeration, the cavitation model of Singhal et al. [6] is employed in Simerics-MP+. This model incorporates real liquid properties, cavitation, aeration, and liquid compressibility. The cavitation vapor distribution is given by the following formulation:

$$\frac{\partial}{\partial t}\int_{\Omega(t)} \rho f_v d\Omega + \int_{\sigma} \rho((v - v_\sigma).n) f_v d\sigma = \int_{\sigma} (D_{f_v} + \frac{\mu_c}{\sigma_{f_v}})(\nabla f_v.n) d\sigma + \int_{\Omega} (R_e - R_c) d\Omega \quad (5)$$

Here, f_v denotes the vapor volume fraction of the working fluid, D_{f_v} is the diffusivity of the vapor mass fraction, and σ_{f_v} is the turbulent Schmidt number. In this work, D_{f_v} and σ_{f_v} are taken to be equal to the mixture viscosity and unity, respectively. The vapor generation rate R_e and the condensation rate R_c are defined as:

$$R_e = C_e \frac{\sqrt{K}}{\sigma_l} \rho_l \rho_v \left(\frac{2}{3} \frac{(p - p_v)}{\rho_l} \right)^{1/2} (1 - f_v - f_g) \quad (6)$$

$$R_c = C_c \frac{\sqrt{K}}{\sigma_l} \rho_l \rho_v \left(\frac{2}{3} \frac{(p - p_v)}{\rho_l} \right)^{1/2} f_v \quad (7)$$

with model constants $C_e = 0.02$ and $C_c = 0.01$. The mixture density is then obtained from:

$$\frac{1}{\rho} = \frac{f_v}{\rho_v} + \frac{f_g}{\rho_g} + \frac{1 - f_v - f_g}{\rho_l} \quad (8)$$

The non-condensable gas (NCG) can be treated either as a purely free gas or as a combination of free and dissolved gas. Simerics-MP+ provides several models that account for both contributions of NCG; further details are given in the software manual [7]. For this simulation, the equilibrium dissolved gas model is adopted, where it assumes that the mass fraction of the total non-condensable gas remains constant, but a part of it is dissolved into the liquid to instantly satisfy the local equilibrium condition.

The governing equations are discretized using the finite volume method and solved with a pressure-based algorithm. Spatial discretization uses a second-order upwind scheme, while time integration is performed with a second-order explicit scheme. The pressure–velocity coupling is resolved using the SIMPLE-S (Semi-Implicit Method for Pressure Linked Equations–Simerics) algorithm [8, 9].

4.2 Translational dynamics model for collisions involving multiple bodies

Simerics-MP+ incorporates a rigid-body motion model that neglects fluid–structure interaction. This class of motion is governed by the linear momentum conservation equation for translational rigid-body dynamics.

The resulting governing equation from linear momentum conservation is

$$m\frac{d^2s}{dt^2} = F_{hydrodynamic} - F_{damping} - F_{spring} - F_{friction} + F_{penalty} \quad (9)$$

Within Simerics-MP+, this equation is solved for the displacement of the moving body simultaneously with the flow and cavitation governing equations.

Here, m denotes the mass of the moving body, and s is its displacement under the net force. $F_{hydrodynamic}$ is the hydrodynamic load arising from pressure and shear stresses. $F_{damping}$ is a damping force that can originate from a spring (if present) or any other external damping device. F_{spring} is the spring force, generally opposing the motion, and $F_{friction}$ is the frictional resistance due to contact between the moving and stationary components. $F_{penalty}$ is an additional force activated upon detection of body–body contact and is expressed as

$$F_{penalty} = kx - cv_{rel} \quad (10)$$

where k is the spring constant, typically chosen as a relatively large positive value, and x is the overlap between bodies, usually on the order of nm. The damping term, given by the product of the damping coefficient c and the relative velocity v_{rel}, serves to reduce jitter or oscillations during impact events.

4.3 Model details

The computational mesh used in this work is shown in figure 5a. At the inlet of the slack adjuster, the pressure is prescribed to vary cyclically over time (see figure 5c). This periodic pressure excitation drives the motion of the valve bodies, leading to their interaction and impact with one another as well as with the three adjacent walls depicted in figure 5a. The configuration also comprises a spring-loaded accumulator, which is charged during phases of elevated inlet pressure, and a drain port that allows fluid to flow in or out depending on the Body 3 displacement. A zoomed-in representation of the

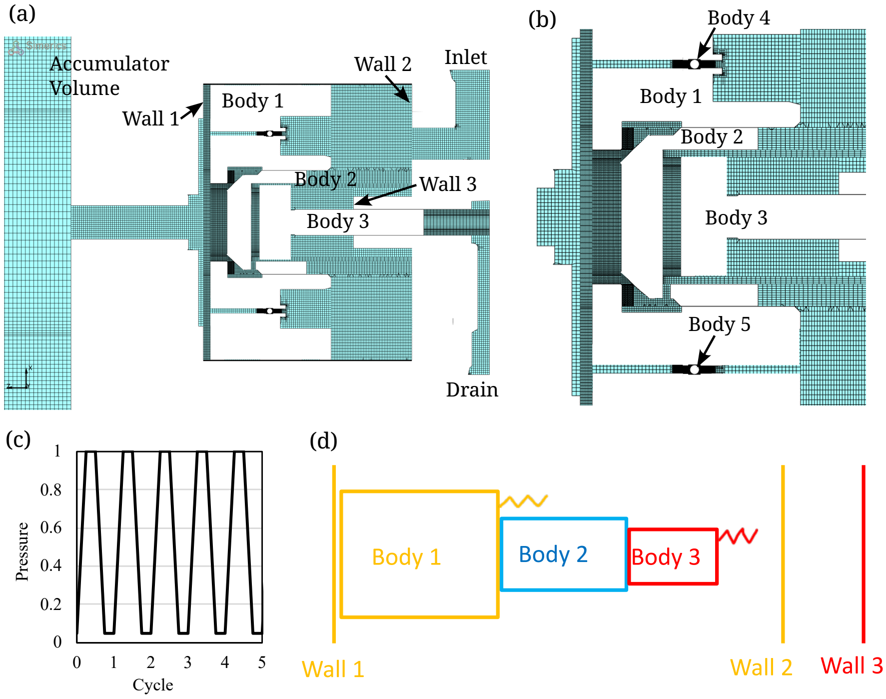

Figure 5 (a) Full CFD mesh showing the accumulator, inlet and drain ports and the valve bodies. (b) Magnified view showing valve bodies and the corresponding deforming zones. (c) Cyclical pressure applied at the inlet. (d) Free-body diagram of the valve bodies represented in 1D for collision modeling.

valve bodies is provided in figure 5b. The ball valves (Body 4 and Body 5) allow flow exclusively from the inlet toward the accumulator. As a result, during the high-pressure inlet phase they facilitate charging of the spring-loaded accumulator, while during the low-pressure inlet phase they prevent any reverse flow from the accumulator back into the inlet.

To simulate collisions among valve components, we represent the 3D bodies and walls using a 1D abstraction, as shown in figure 5d. During operation, the Body 1, Body 2, and Body 3 may impact each other. The Body 1 and Body 3 are preloaded by springs. The Body 1 is constrained by wall 1, wall 2 and the Body 2. The Body 2 is constrained by the Body 1 and the Body 3. The Body 3 is constrained by the Body 2 and wall 3. Because the positions of the valve bodies are mutually dependent, we employ the penalty method

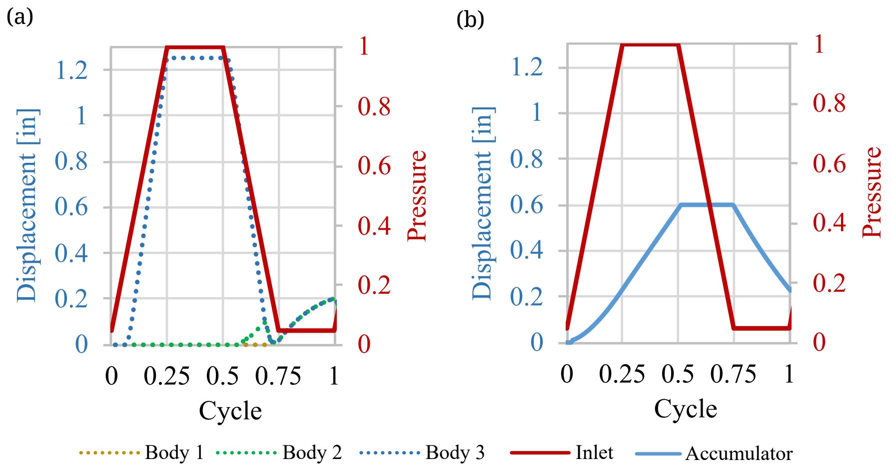

Figure 6 (a) Valve bodies' displacements from their resting positions and (b) accumulator displacement as a function of time for the initial cycle. Inlet pressure applied during the simulation is shown in the secondary-y for reference. Time is non-dimensionalized using cycle time and pressure is normalized by the highest pressure used in the inlet.

(see eqn. 10) to decouple them into individual free-body diagrams, each with its corresponding force balance (see eqn. 9).

4.4 Results and discussion

In this section, we analyze the outcomes of the 3D CFD simulation to gain a detailed understanding of the system using the desig finalized during the 1d analysis. As described in the previous section, a pressure pulse is applied at the inlet pressure boundary. This pressure varies cyclically and reflects the actual operating conditions of the slack adjuster.

During the initial cycle of inlet pressure variation, as the inlet pressure increases, Body 3 is driven toward wall 3, as illustrated in the displacement plot in figure 6a, because the fluid force exceeds the restoring force of the spring attached to Body 3. This behavior can be observed more distinctly in the contour plots in figure 7a,b,c. Over this period, the accumulator becomes fully charged, which is indicated by its displacement rising to the maximum value, as shown in figure 6b.

During the inlet pressure ramp-down phase of the first cycle, the spring force acting on Body 3 exceeds the fluid pressure, causing it to move away from wall 3. This behavior is quantified in figure 6a and illustrated in fig-

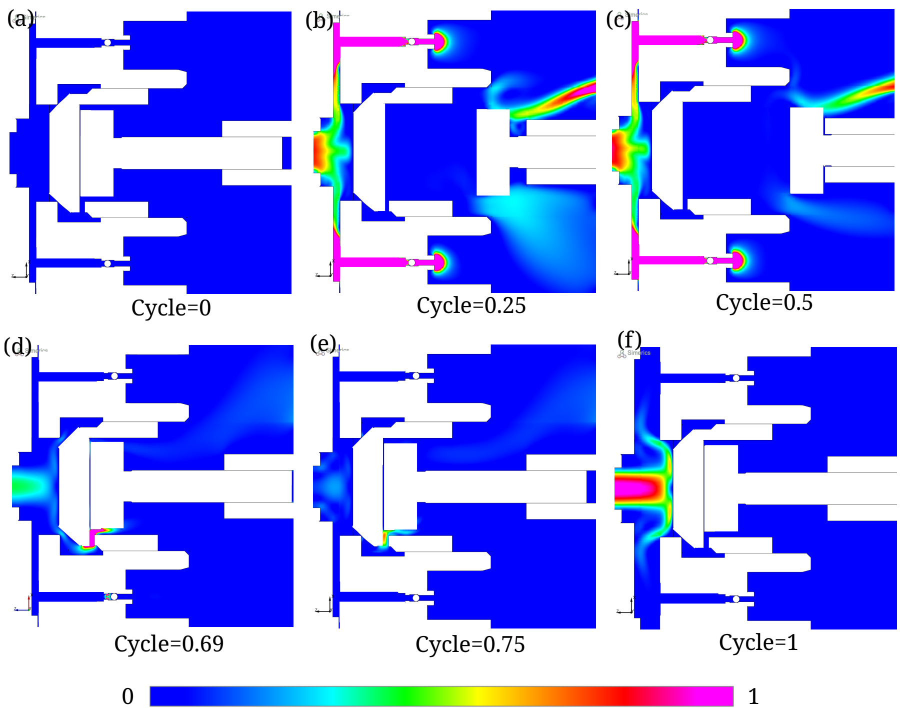

Figure 7 (a-f) 3D contour of velocity magnitude showing the valve body movements for different times in the initial cycle. The velocities are in ms^{-1}.

ures 6d and e. During this interval, the accumulator discharges (see figure 6b) because its pressure is higher than that at the inlet. As the ball valve restricts direct flow from the accumulator to the inlet, the fluid instead drives Body 2, separating it from Body 1 and creating a new flow path from the accumulator to the inlet through the gap that opens between bodies 1 and 2. This is reflected in figure 6a, where Body 2 begins to move approximately Cycle=0.6, and is further depicted in the contour plot figure 7d. This sequence of events puts bodies 2 and 3 on a collision trajectory. At around Cycle=0.69, they collide and Body 3 forces Body 2 back toward Body 1, thereby closing the flow channel formed between bodies 1 and 2. figure 6e provides a detailed visualization of this event. Once this leakage path is eliminated, the outflow from the accumulator begins to displace all bodies at approximately Cycle=0.75, continuing until the end of the cycle. The final positions of the valve bodies at the end of the first cycle are shown in figure 7f.

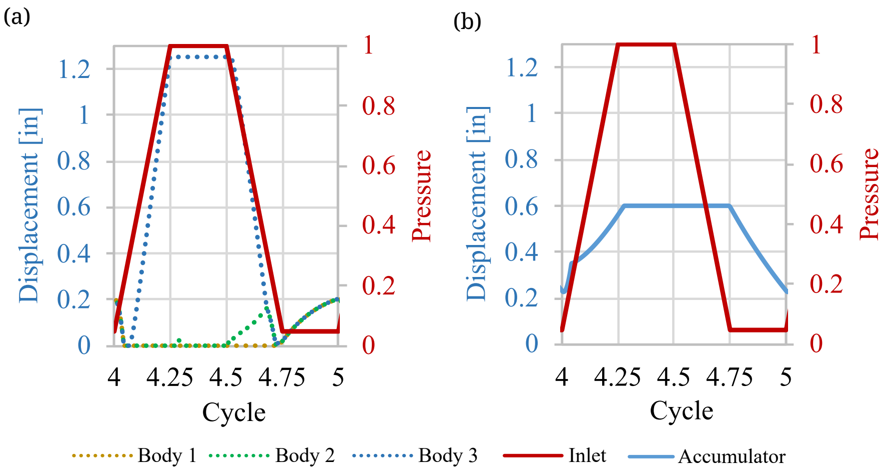

Figure 8 (a) Valve bodies' displacements from their resting position and (b) accumulator displacement as a function of time for the final cycle. Inlet pressure applied during the simulation is shown in the secondary-y for reference. Time is non-dimensionalized using cycle time and pressure is normalized by the highest pressure used in the inlet.

After the first cycle, the accumulator is primed and the behavior of the valve bodies and the accumulator in the subsequent cycles is periodic. Hence, we look at the results of the last inlet pressure cycle we simulated. Unlike the first cycle, the valve bodies and accumulators are not in their resting position, but offset by some distance from the wall 1, which coincides with the end state of the first cycle. This can observed by comparing the valve body and accumulator positions in the initial cycle figure 6 and the final cycle figure 8. As the inlet pressure ramps up, the increasing inlet pressure combined with the spring force pushes the valve bodies 1, 2 and 3 closer to the wall 1 ie. toward their resting positions like evident in the figure 8a. Like the first cycle, once the inlet pressure increases enough to overcome the spring of the Body 3, the Body 3 starts to move towards the wall 3 as illustrated in the figures 8b,c. Unlike the first cycle (figure 6), the accumlator gets fully charged very early in the high pressure phase in the final cycle (figure 8b). Consequently, Body 2 starts moving earlier as seen in the figure 8a.

During the ramp-down stage of the final cycle, Body 3 returns to its original position as the spring force overtakes the fluid force. As Body 3 moves back, it collides with Body 2, pushing it toward Body 1 and thus closing the leakage path between Bodies 1 and 2. The contour plots in figure 9d,e,f

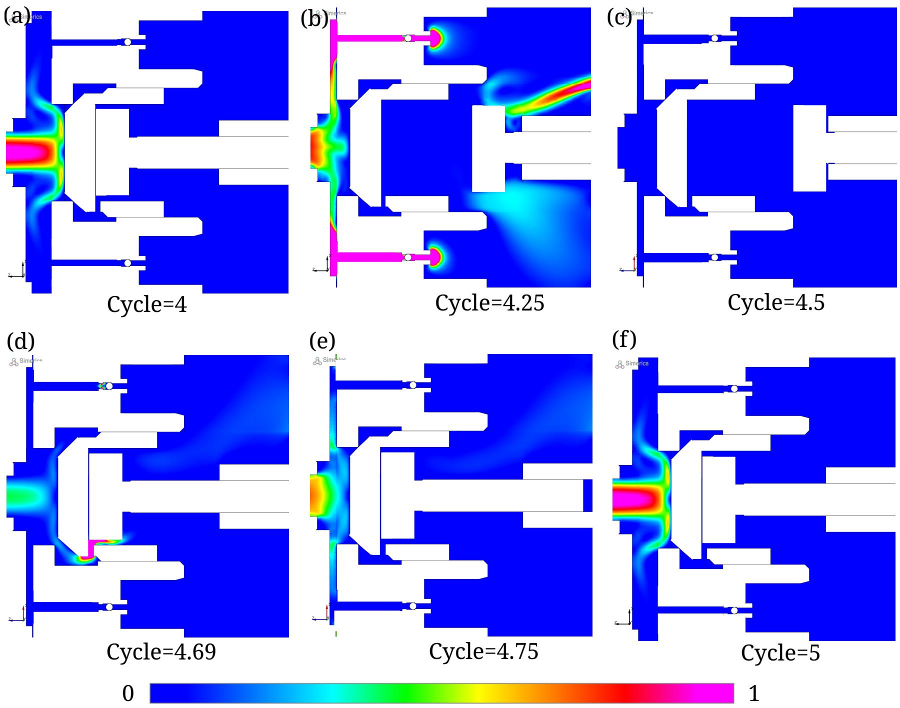

Figure 9 (a-f) 3D contour of velocity magnitude showing the valve body movements for different times in the final cycle. The velocities are in ms^{-1}.

qualitatively illustrate this behavior, and figure 8 shows the corresponding quantitative results. This mechanism is analogous to that observed in the initial cycle, with the key difference that in the later cycles Body 2 travels a greater distance from its starting position because the accumulator is charged more quickly. As in the first cycle, all the valve bodies are displaced toward wall 3 by a certain amount. After this, the entire sequence repeats periodically.

5 Comparison of 1d and 3d simulations

It should be emphasized that the quantitative results reported for the 1D and 3D simulations are not in agreement. For example, the valve body displacements obtained from the 1D simulations, shown in figure 3, differ from the displacements predicted by the 3D simulations, which are presented in figures. 6 and 8. The 3D methodology solves the full flow field and explicitly accounts for turbulence and cavitation, effects that are not included in the 1D model. As a result, the opening and closing times of the valve bodies can differ significantly between the two approaches. In a complex valve system such as this, even small variations in timing can lead to large differences in the overall displacements.

Nonetheless, the global system behavior is comparable in both approaches. For instance, accumulator priming during the first cycle is captured in both the 1D and 3D simulations. Another example is Body 3 driving Body 2 to close the leakage path between the valve bodies, followed by the subsequent motion of all valve bodies; this sequence is observed in both the 1D and 3D results, as illustrated in figures. 7 and 8, respectively.

6 Industrial Impact

Typical new-product development (NPD) workflows in the off-highway hydraulics industry can stretch for many months or years, and require 1-3 prototyping and "testbed" builds to validate novel elements. These prototypes and testbeds consume resources at an accelerated rate relative to increased novelty in design. Conservatively, organizational resource impact may be 50,000 USD or more for a prototype or testbed with significant new component design validation. In addition, some phenomena are difficult or impossible to observe during physical testing. In the present case, equipment, time, instrumentation, and personnel limitations put full validation of unconstrained edge-case poppet motion out of reach. Typically, valuable time is consumed on adjusting validation goals and plans to mitigate for resource constraints and missing or compromised data, which in turn weakens support of needed qualitative and quantitative design inferences, leading to mixed results or extensive post-processing.

In the study presented here, a fraction of typical prototyping and test resources were needed, and these resources were targeted on risk areas that would be exceedingly difficult to observe and manipulate in physical testing. Rapid post-processing and direct comparisons of simulation results fully supplanted typical pre-launch prototyping cycles. This team anticipates the launch program will proceed directly to testing First Article parts from a production-intent supply chain.

7 Conclusion

A well-planned simulation strategy should enable ambitious concept development even in mature hydraulic components and systems. A decoupled 1D–3D approach is especially effective: 1D models support rapid ideation, subsystem/system studies, and fast DoE to explore edge cases and failure drivers, while 3D simulations provide high-fidelity insight into component-level physics and application behavior.

Using each tool where it fits in the design cycle reduces development time and minimizes late-cycle surprises during testing. The available simulation tools can replace portions of early prototyping - when risk and design churn are highest - while enabling teams to evaluate concepts that would be difficult to assess with traditional methods. Model fidelity can be increased incrementally as the design matures, focusing effort on the highest-risk elements with clear requirements and validation criteria.

Finally, linking 3D visuals and results with 1D system behavior improves communication across cross-functional teams and brings Subject Matter Experts into design reviews and Design Failure Mode and Effect Analysis discussions earlier, leading to more efficient and effective pre-production verification testing.

References

[1] T. H. Engle, "Hydraulic slack adjuster and brake circuits therefor," May 11 1976. US Patent 3,955,370.
[2] F. W. Berwanger, "Aircraft brake piston hydraulic adjuster assembly," Jan. 23 1996. US Patent 5,485,902.
[3] R. E. Landgraf, "Automatic brake adjuster mechanism," June 1 1971. US Patent 3,581,849.
[4] M. A. Salam, *Hydraulic Cylinders*, pp. 257–286. Singapore: Springer Singapore, 2022.
[5] J. F. Blackburn, G. Reethof, and J. L. Shearer, "Fluid power control," *(No Title)*, 1960.
[6] A. K. Singhal, M. M. Athavale, H. Li, and Y. Jiang, "Mathematical basis and validation of the full cavitation model," *Journal of Fluids Engineering*, vol. 124, no. 3, pp. 617–624, 2002.
[7] Simerics Inc., "Simerics-MP+ user manual," 2024.
[8] A. Pandey, J. Wang, D. Maiti, and Y. Jiang, "Performance and validation of a segregated pressure-based solver for computations of low and high-speed compressible flows," in *AIAA SCITECH 2023 Forum*, p. 2274, 2023.
[9] S. Taghizadeh, K. C. Ng, J. Horen, and S. Dhar, "A 3d computational fluid dynamics and acoustics simulation approach for noise mitigation prediction in gerotor pumps," tech. rep., SAE Technical Paper, 2024.